Intrinsic excitability mechanisms of neuronal ensemble formation

Tzitzitlini Alejandre-García, Samuel Kim, Jesús Pérez-Ortega and Rafael Yuste

Neurotechnology Center, Dept. Biological Sciences, Columbia University, New York, NY 10027, USA

Running Head: Mechanisms of neuronal ensembles

Correspondence to:
Tzitzitlini Alejandre-García
902 NWC Building 550 West 120 Street, Box 4822, New York, NY, 10027.
Email: at3415@columbia.edu

Conflict of Interest: The authors declare no competing financial interests

Acknowledgments: We thank James Holland, for his assistance and members of the Yuste Lab for useful comments. Supported by R01EY011787 and R01MH115900. R.Y. is an Ikerbasque Research Professor at the Donostia International Physics Center (DIPC). The authors have no competing financial interests to declare. S.K. and R.Y. conceived the project. S.K. and T.A. performed experiments and T.A. and R.Y. wrote the paper. T.A., S.K. and J.P. analyzed the data. All authors planned experiments, discussed results and edited the paper. R.Y. assembled and directed the team and secured funding and resources.

Abstract

Neuronal ensembles are coactive groups of cortical neurons, found in both spontaneous and evoked activity, which can mediate perception and behavior (Cossart et al., 2003; Buzsáki, 2010; Carrillo-Reid et al., 2019; Marshel et al., 2019). To understand the mechanism that lead to the formation of neuronal ensembles, we generated optogenetically artificial photo-ensembles in layer 2/3 pyramidal neurons in brain slices of mouse visual cortex from both sexes, replicating an optogenetic protocol to generate ensembles *in vivo* by simultaneous coactivation of neurons (Carrillo-Reid et al. 2016). Using whole-cell voltage-clamp recordings from individual neurons and connected pairs, we find that synaptic properties of photostimulated were surprisingly unaffected, without any signs of Hebbian plasticity. However, extracellular recordings revealed that photostimulation induced strong increases in spontaneous action potential activity. Using perforated patch clamp recordings, we find increases in neuronal excitability, accompanied by increases in membrane resistance and a reduction in spike threshold. We conclude that the formation of neuronal ensemble by photostimulation is mediated by cell-intrinsic changes in excitability, rather than by Hebbian synaptic plasticity or changes in local synaptic connectivity. We propose an “iceberg” model, by which increased neuronal excitability makes subthreshold connections become suprathreshold, increasing the functional effect of already existing synapses and generating a new neuronal ensemble.

Introduction

The function of brain is anchored on the activity of groups of connected neurons, forming microcircuits (Schüz and Braitenberg, 2001; Shepherd, 2004). These groups of coactive neurons, or ensembles (also known as assemblies or attractors), exhibit synchronous or correlated activity (Lorente De Nó, 1938; Hebb, 1949; Hopfield, 1982; Abeles, 1991; Cossart et al., 2003; Buzsáki, 2010; Miller et al., 2014; Yuste, 2015; Carrillo-Reid et al., 2016, 2019; Marshel et al., 2019), and appear critical for brain function (Hoshiba et al., 2017) and memory formation (Hebb, 1949). In the cerebral cortex, these states may arise from patterns of multineural activity that persist spontaneously after an initial stimulus, generating recurrent activity (reverberations) (Lorente de Nó, 1933; Churchland and Sejnowski, 1992). Cortical ensembles correlate with different functions of the animal, not just memory storage, but also representation of thoughts, and percepts as demonstrated in the primary visual cortex of awake mice during spontaneous and visually evoked activity patterns in neurons (Miller et al., 2014a; Carrillo-Reid et al., 2019; Marshel et al., 2019). Moreover, the disorganization of neuronal ensembles is associated with neuropsychiatric disorders such as schizophrenia (Hamm et al., 2017).

One hypothesis of how an ensemble could be formed was first proposed by Donald Hebb in 1949. According to this rule, the persistent and repeated activation of connected neurons induce metabolic changes or growth of processes in one or both cells that strengthens those connections. One mechanism that fulfills Hebb's rule is Long-Term Synaptic Potentiation (LTP), originally defined as a long-lasting increase in synaptic efficacy after a high frequency burst electrical stimulation (Bliss and Gardner-Medwin, 1973). Accordingly, changes in synaptic weights produces preferential connectivity that controls the flow of activity within and between neuronal ensembles (Hoshiba et al., 2017). Since its initial discovery (Bliss and Gardner-Medwin, 1973), LTP has been widely established as the cellular correlate for memory and learning. Indeed, recent

50 studies have supported the idea that Hebbian plasticity could underlie ensemble formation *in vivo*
51 (Carrillo-Reid et al., 2016), since the two-photon optogenetic synchronous stimulation of a groups
52 of neurons 50 to 100 times bound them together into an imprinted ensemble which become
53 spontaneously coactive. Therefore, co-activation of a group of neurons in awake mice can create
54 a new stable artificial ensemble (Carrillo-Reid et al., 2016). This result is consistent with the
55 Hebbian hypothesis on the formation of neuronal ensembles, but no direct evidence has yet been
56 presented to demonstrate that the formation of ensembles depends on changes in synaptic
57 connections in neuronal circuit.

58 As an alternative hypothesis, experimental evidence has revealed widespread activity-dependent
59 cell-intrinsic mechanisms in cortical circuits (Ryan et al., 2015; Titley et al., 2017). This suggests
60 that the formation and stability of an ensemble could be carried out by cell-autonomous intrinsic
61 mechanisms (Abraham et al., 2019). This hypothesis is consistent with experiments where the
62 activation of specific patterns of cellular activity in hippocampus recalls stored memories, even
63 under treatment with protein synthesis inhibitor which should prevent LTP (Ryan et al., 2015;
64 Tonegawa et al., 2015). Moreover, Purkinje cells can acquire and represent a specific input with
65 a temporal pattern of activity, suggesting that patterns of activity may be imprinted intrinsically by
66 the neurons itself (Johansson et al., 2014). Thus, changes excitability state of the neurons may
67 contribute to ensemble consolidation, rather than the reinforcement of its synapses, as Hebb
68 proposed (Disterhoft and Oh, 2006; Pignatelli et al., 2019).

69 In order to test these alternative mechanisms of ensemble formation. we built photo-ensembles
70 in mouse neocortical slices, following an *in vivo* optogenetic protocol (Carrillo-Reid et al., 2016).
71 We then directly measured electrophysiological properties of photostimulated neurons, finding a
72 lack of changes of synaptic properties yet generalized increases in cell-intrinsic excitability. We
73 conclude that ensemble formation is a non-Hebbian phenomenon.

74 **Materials and Methods**

75 All procedures were performed in accordance with the U.S. National Institutes of Health and
76 Columbia University Institutional Animal Care and Use Committee guidelines. Experiments were
77 carried out on C57BL/6 transgenic mice (Vglut1-Cre, Jackson Laboratories;
78 RRID:IMSR_JAX:00064) of both sexes at postnatal day of 1 - 2 months. Animals were housed on
79 a 12h light-dark cycle with food and water ad libitum.

80 **Viral injection**, after 1 month postnatal, animals were anesthetized with 2% isoflurane on a
81 headfiexed stereotactic apparatus. After sterilizing the incision site, the skin was opened and,
82 using an FG 1/4 dental drill, a small hole goes thin in the skull over visual primary cortex (2.5 mm
83 lateral and 0.3 mm anterior from the lambda, 200 µm from pia). We injected 300 nL of virus at a
84 rate of 30-40 nL/s, using a microsyringe pump (Micro 4), a Hamilton 7653-01 and a glass pipette.
85 Once pipette was placed, we waited 5 min before and after virus injection and finally closing the
86 scalp with sutures. Viruses injected were: Cre-dependent AAV-CAG-DIO-ChroME-P2A-H2B-
87 mRuby3 (Addgene viral prep # 108912-AAV9) or AAVDJ-CaMKIIa-C1V1(E162T)-TS-p2A-EYFP-
88 WPRE (Stanford University Gene Vector and Virus Core). Mice were used for electrophysiology
89 experiments 2–3 weeks postinjection.

90 **Brain slices**, mice were anesthetized with ketamine/xylazine. After transcardiacal perfusion
91 procedure and posterior cervical dislocation, brain sagittal slices were obtained as described (Ting
92 et al., 2018). The brains were quickly dissected and cooled in a continuously gassed (95% O_2 and
93 5% CO_2) icy NMDG-HEPES artificial cerebrospinal fluid (aCSF). Transcardiacal perfusion and
94 cutting solution, containing (in mM): 92 NMDG, 2.5 KCl, 1.25 NaH_2PO_4, 30 $NaHCO_3$, 20 HEPES,
95 25 glucose, 2 thiourea, 5 Na-ascorbate, 3 Na-pyruvate, 0.5 $CaCl_2$, and 10 $MgS0_4$ with pH titrated
96 to 7.3–7.4 with HCl, or 222 Sucrose, 2.6 KCl, 27 $NaHCO_3$, 1.5 NaH_2PO4, 2 $MgSO_4$, and 2 $CaCl_2$.
97 300 μm thick sagittal slices were cut on a Leica VT1200 S vibratome (Leica Biosystems) and

allowed to recover for 20 min at 34°C HEPES holding aCSF solution (in mM): 92 NaCl, 2.5 KCl, 1.25 NaH_2PO_4, 30 $NaHCO_3$, 20 HEPES, 25 glucose, 2 thiourea, 5 Na-ascorbate, 3 Na-pyruvate, 2 $CaCl_2$, and 2 $MgSO_4$. Titrate pH to 7.3–7.4 with NaOH. Finally, slices were transferred to aCSF containing the following (in mM): 124 NaCl, 2.5 KCl, 1.25 NaH_2PO_4, 24 $NaHCO_3$, 12.5 glucose, 5 HEPES, 2 $CaCl_2 \cdot 2H_2O$, and 2 $MgSO_4 \cdot 7H_2O$ with pH titrated to 7.3-7.4, or 126 NaCl, 3 KCl, 1.145 NaH_2PO_4, 26 $NaHCO_3$, 10 Glucose, 2 $MgSO_4$, and 2 $CaCl_2$. Slices rested in dark for at least 1 hr before use.

Patch Clamp Recordings. Brain slices were carefully placed in the recording chamber on an upright microscope (Olympus, BX50WI), they were continuously perfused with gassed (95% O_2 and 5% CO_2) aCSF at 5 ml/min. All electrophysiological recordings were performed using patch pipettes, made from borosilicate glass (World Precision Instruments), pulled with a micropipette puller (DMZ-Universal puller), in order to get 4 – 6 MΩ as final resistances.

For whole-cell, patch pipettes were filled with intracellular solution containing the following (in mM): 130 K-gluconate, 20 KCl, 10 HEPES, 10 Na_2-phosphocreatine, 4 Mg-ATP, 0.03 Na_2-GTP, and titrated to pH 7.3 with KOH, or 135 K-$MeSO_4$, 5 KCl, 5 HEPES, 0.5 EGTA, 10 Na_2-phosphocreatine, 2 Mg-ATP, 0.5 Na_2-GTP, and titrated to pH 7.3 with KOH. For cell-attached, pipettes were filled with aCSF solution. For perforated patch clamp, pipette solution containing: 130 K-gluconate, 20 KCl, 10 HEPES, 2 $MgCl_2$, 4 Mg-ATP, 0.03 Na_2-GTP, and titrated to pH 7.3 with KOH. 50 – 100 ng/ml gramicidin (sigma Aldrich) dissolved in dimethyl sulfoxide (DMSO). To allow membrane sealing, the tip was immersed in clean pipette solution and then the pipette was back-filled with gramicidin containing solution.

In each case, the patch pipette was placed in contact with the cell with the aid of a SM-5 micromanipulator (Luigs & Neumann). Stimulation and data acquisition were sampled at 10 kHz and low pass filtered at 4kH using a Multiclamp 700B amplified (Molecular Devices) and Im-

122 Patch© open access software http://impatch.ifc.unam.mx . Recordings were continued when leak
123 current while < 25 pA or seal resistance > 1 GΩ. Recordings were analyzed with custom routines
124 in MATLAB.

125 **Imaging**. To identify the target brain region, we used an upright microscope with a 4X/0.10 NA
126 air objective (Olympus) before switching to 60X/0.90 W NA water immersion objective to confirm
127 ChroME or C1V1 opsin expression on target cells. For ChroME, the mRuby3 fluorescent reporter
128 was excited with monochromatic light transmitted through fiber optics into the microscope
129 (Olympus 100 w high pressure mercury burner model BH2RFLT3). Emitted fluorescence was
130 bandpassed with an Olympus U-49006 ET CY5 filter set: 620/60 ex, 520 dichroic mirror, and
131 700/75 em. For C1V1, the EYFP fluorescent reporter was visualized via a 500/24 excitation filter
132 (Semrock), 520 dichroic mirror (Semrock), and 542/27 emission filter (Semrock). Fluorescence
133 images were acquired (50 ms exposure; 10 Hz) using a camera (Orca-ER C4742-95,
134 Hamamatsu) and shutter UNIBLITZ model VCM-D1 controlled by HC Image software
135 (Hamamatsu). We visualized individual neurons' fluorescence deep (100 μm) into the brain slice
136 exhibiting a clear L2/3 distinction, taken as evidence of C1V1 or mRuby3 as Cre promoter-driven
137 expression.

138 **Photostimulation**. Optogenetic photostimulation of ChroMe opsin was performed using a 470
139 nm fiber-coupled LED (M470F1, Thorlabs), fiber optic cannula (M79L01, Thorlabs) and LED driver
140 (M00329012, Thorlabs) , while photostimulation of C1V1 was performed using a 617 nm fiber-
141 coupled LED (M617F2, Thorlabs), fiber optic cannula (CFM14L10, Thorlabs) and LED driver
142 (DC2200, Thorlabs). The photostimulation protocol aimed to mimic stimulation conditions used in
143 previous *in vivo* experiments (Carrillo-Reid et al., 2016), in order to build artificial photo-
144 ensembles. This photostimulation protocol consisted of trains of 10 Hz, 5 ms light pulses for 4 s
145 followed by a 10 s rest.

146 Only neurons that exhibited action potentials or action currents in response to each LED pulse
147 were included in the data analysis. Moreover, LED intensity applied throughout the protocol was
148 the lowest necessary for induce action potentials or action currents. This procedure was carried
149 out for every recording both photostimulated and unstimulated neurons (controls). For
150 photostimulated neurons, the parameters were always monitored before and after ongoing
151 photostimulation protocol (15 to 80 min). Photostimulation protocol was stopped every 15 or 20
152 min to monitor the parameters and then it was restarted. For unstimulated neurons, the same
153 parameters were monitored at the beginning and then every 15 – 20 min until approximately 80
154 min after no photostimulation.

155 **Experimental design.** To generate photoensembles (Carrillo-Reid et al., 2016), we delivered
156 Cre-dependent ChroME opsin (Mardinly et al., 2018), with virus injection in transgenic VGlu1-Cre
157 mice, or C1V1 opsin in wild-type mice. No significant differences were found in experiments with
158 both opsins and data were pooled together. Then, we localized the L2/3 pyramidal neurons in
159 primary visual cortex of brain slices expressing ChroME or C1V1 (Figure 1A). Then, in order to
160 test whether the maintenance of an imprinted photo-ensemble was due to reinforcement of
161 synaptic connections among the neurons (Carrillo-Reid et al., 2016) or by cell-intrinsic regulation
162 (Pignatelli et al., 2019), we recorded and characterized passive and active electrical properties of
163 the neurons using whole-cell, cell-attached and perforated patch-clamp recording of at least, two
164 pyramidal neurons simultaneously *in vitro* (Figure 1B).

165 Once we obtained a patch, we compared cellular electrical properties before and after build the
166 artificial photo-ensembles with the photostimulation protocol. For whole-cell recordings, we
167 examined changes in evoked EPSCs and spontaneous EPSCs (sEPSCs) in response to
168 photostimulation (Figure 1C); for cell-attached recordings we measured changes in spontaneous
169 firing throughout the photostimulation (Figure 1D); for perforated patch clamp we explored

170 parameters like membrane resistance, rheobase, firing rate and the phase of action potentials
171 (Figure 1E).

172 **Statistical Analysis**. Statistical details are showing in each figure legends. In general, group data
173 are expressed as mean ± sem. Shapiro-Wilk was used for normality test. Student's unpaired or
174 paired t test were used for comparing parametric groups. Wilcoxon rank-sum and Mann-Whitney
175 test were used for nonparametric analysis. Differences between two groups were considered
176 significant when $*p < 0.05$, $**p < 0.01$ and $***p < 0.001$. All statistics were performed using
177 statistical functions in MATLAB.

178

179 **Results**

180 **Lack of synaptic plasticity between photostimulated neurons**

181 Our initial hypothesis, based on our previous results photo-imprinting ensembles *in vivo* (Carrillo-
182 Reid et al., 2016), was that neuronal ensembles are built by Hebbian synaptic plasticity due to
183 the simultaneous activation of pre and postsynaptic neurons. Thus, new ensembles could be
184 formed by the creation of new synaptic connections or reinforcement or potentiation of existing
185 ones. To explore this we first tested whether persistent and repeated optogenetic activation of
186 connected neurons induced synaptic plasticity in one or both cells (Hebb, 1949; Cossell et al.,
187 2015). In order to answer this question, we performed dual whole-cell recordings from adjacent
188 neurons, which are more likely to be connected (Ko et al., 2011), of L2/3 pyramidal neurons
189 expressing the opsins ChroME or C1V1 in cortical slices from adult animals (Figure 2A). Using
190 patch clamp, we recorded simultaneously from pairs of neurons searching for monosynaptic
191 connections in both directions (n = 5, 4 mice for photostimulated group and n = 5, 3 mice for
192 unstimulated). For measuring membrane potential, we performed current-clamp recordings,
193 injecting necessary current (between -10 to 10 pA) to keep neurons at -70 mV, close to their
194 resting membrane potential. Under these conditions, we induced action potentials in presynaptic
195 neurons with 10 current depolarizing pulses at the lowest intensity (amplitude: 400 to 600 pA, 2
196 ms, 20 Hz trains). For measuring synaptic currents, postsynaptic neurons were recorded in
197 voltage-clamp at a holding potential of -70 mV. This membrane potential prevents the generation
198 of voltage-dependent currents, and better isolate EPSCs. We classified connections as
199 monosynaptic if EPSC latency was <2 ms relative to its corresponding presynaptic spike (Figure
200 2B; n = 10, 7 mice). We included in the analysis only cells that exhibited detectable EPSCs at the
201 beginning and end of the recording, which lasted roughly 60 min, including the photostimulation.
202 To confirm the stability in the connection until the end of the recording, we averaged 30

203 postsynaptic traces, showing 10 EPSCs elicited by the presynaptic train before and after
204 photostimulation for a representative neuron (Figure 2C).

205 In these pairs of connected neurons, we examined if optogenetic photostimulation induced
206 synaptic changes. Visual inspection failed to reveal any major alterations in EPSCs. To quantify
207 this, we calculated the paired-pulse ratio (PPR), i.e. the ratio of amplitudes for the second to the
208 first EPSC in the train ($EPSC_2/EPSC_1$) of cells before (0.7 ± 0.07 PPR) and after photostimulation
209 (0.8 ± 0.08 PPR; p = 0.2 Wilcoxon rank-sum; n = 5, 4 mice) and compared it with a control group
210 of unstimulated neurons before (0.75 ± 0.03 PPR) and after 30 min (0.7 ± 0.1 PPR; p = 0.7
211 Wilcoxon rank-sum; n = 5, 3 mice) (Figure 2D). No significant differences were observed in PPR
212 of evoked EPSC when we compared the changes in PPR of photostimulated (-0.12 ± 0.04,
213 change in PPR) versus unstimulated neurons (0.1 ± 0.1 change in PPR; p = 0.5 Mann Whitney's).
214 Moreover, average peak currents of the first EPSC1 ($EPSC_1$) of photostimulated neurons showed
215 no difference before (24 ± 9 pA) and after photostimulation (21 ± 10 pA; p = 0.6 Wilcoxon rank-
216 sum; n = 5, 4 mice), similarly to unstimulated neurons before (15 ± 2 pA) and after 30 min (9 ± 2
217 pA; p = 0.06 Wilcoxon rank-sum; n = 5, 3 mice). The average change comparison between
218 photostimulated (-4 ± 3 pA change in amplitude) and unstimulated neurons (-2 ± 2 pA change in
219 amplitude) were also not statistically different (p = 0.5, Mann Whitney's; Figure 2E). We concluded
220 that synaptic plasticity was not altered after photostimulation. Our results suggest that, under our
221 conditions, synaptic plasticity among connected neurons did not contribute to build photo-
222 ensembles.

223

224 **Lack of changes in spontaneous synaptic inputs in photostimulated neurons**

225 The previous results did not rule out the possibility that synaptic plasticity among non-connected
226 or non-recorded neurons contributed to the generation of photoensembles. To search for

227 evidence of synaptic plasticity in the neuronal population, we measured spontaneous EPSCs from
228 recorded neurons and compared them before and after optogenetic stimulation (Figure 3A). Since
229 the viral vector labels pyramidal cells extensively, we reasoned that a significant portion of a given
230 cell's presynaptic partners would also express ChroME or C1V1 and, thus, fire in response to
231 photostimulation. If this leads to synaptic potentiation in the connections, we would expect to
232 detect it as changes in amplitude of spontaneous EPSCs.

233 To test this, we recorded spontaneous EPSCs from connected and unconnected neurons. The
234 changes in mean spontaneous EPSC frequency and amplitude were compared between
235 photostimulated (n = 12 pairs, 7 mice) and unstimulated cells (n = 8 pairs, 4 mice). We found no
236 statistically difference in spontaneous EPSCs frequency changes between them (-26 ± 25 % for
237 photostimulated cells and -33 ± 18 % for unstimulated cells; p = 0.4, Mann Whitney's); or any
238 significant differences in spontaneous EPSCs amplitude (-13 ± 8 % for photostimulated cells and
239 -17 ± 8 % for unstimulated cells; p = 0.9, Mann Whitney's) (Figure 3B).

240 We were surprised by that lack of synaptic plasticity after potentiation, and reasoned that synaptic
241 potentiation in connected or unconnected neurons was perhaps masked owing to intracellular
242 washout by prolonged whole-cell recordings. To explore this, we recorded EPSPs using
243 perforated patch clamp from neurons in current clamp, before and after photostimulation, but we
244 also did not observe evidence of new evoked EPSP (n = 6, 3 mice; Figure 3C). Using perforated
245 patch recordings, we also compared the number of spontaneous EPSPs before and after
246 photostimulation (17 ± 2 EPSPs before and 17 ± 2 EPSPs after); instantaneous EPSPs frequency
247 (4.5 ± 0.7 Hz before and 5.7 ± 0.6 Hz after) and EPSPs amplitudes (1.2 ± 0.2 mV before and 1.5
248 ± 0.2 mV after). None of these parameters showed significant differences (p = 0.4; p = 0.4 and p
249 = 0.7 respectively; Wilcoxon's test) (Figure 3D). Thus, both whole-cell and perforated recordings
250 showed a similar lack of detectable changes in evoked or spontaneous synaptic inputs after
251 photostimulation. We concluded that, under our experimental conditions, photostimulation of

252 neurons with the same optogenetic protocols that induce the formation of ensembles *in vivo* did
253 not generate appreciable changes in synaptic properties.

254

255 **Optogenetic stimulation increases neuronal spontaneous activity**

256 During our whole cell recordings, we noticed that photostimulated neurons were often
257 spontaneously coactive. Indeed, close inspection of the *in vivo* data indicated that, after
258 photostimulation, neurons increase their spontaneous activity (Carrillo-Reid et al., 2016). To
259 explore this possibility, we performed cell-attached recordings from neurons in slices to
260 noninvasively investigate the effect of photostimulation on the spontaneous firing rate of neurons.
261 In these experiments, we observed progressive increases in spontaneous firing rate between
262 optogenetic stimuli in 60 % of the neurons (n = 17, 5 mice; Figure 4A). This increase in
263 spontaneous activity persisted for 30 min after photostimulation (3 ± 3 peaks before vs. 49 ± 14
264 peaks after in 60 s window; p = 0.009; Wilcoxon's test). This suggested that photostimulation
265 increase neuronal excitability and it was not simply due to a rebound response after stimulation
266 (Figure 4B).

267 To analyze with more detail this increase in spontaneous activity, the instantaneous firing
268 frequency was measured in 60 s windows. We found significant increases in instantaneous
269 frequency after photostimulation (0.15 ± 0.13 Hz before vs. 2 ± 0.7 Hz after; p = 0.009 Wilcoxon's
270 test; n = 17, 5 mice) (Figure 4C, 4D). But for unstimulated neurons, we found no significant
271 differences in number of spikes (17 ± 8 spikes before vs. 20 ± 10 spikes after; p = 0.2; Wilcoxon's
272 test; n = 14, 2 mice) or instantaneous frequency (4 ± 1.7 Hz before vs. 5 ± 1.8 Hz after; p = 0.3
273 Wilcoxon's test; n = 14, 2 mice) at the beginning and end of recording. This increase in
274 spontaneous activity after photostimulation suggests that repeated photostimulation could
275 increase neuronal excitability.

Photostimulation increases membrane excitability and input resistance

Our results indicated that the formation and stability of a cell ensemble could be mediated by cell-intrinsic increases in cellular excitability (Ryan et al., 2015; Titley et al., 2017; Abraham et al., 2019) rather than by reinforcement of its synapses (Disterhoft and Oh, 2006; Pignatelli et al., 2019). To explore cell-intrinsic mechanisms of ensemble formation, we recorded neurons with perforated patch clamp, before and after photostimulation, quantifying intrinsic electrophysiological parameters such as: current injection firing-dependence, membrane resistance, firing rate, frequency and I-V phase plots.

We first measured the membrane potential response to current injections with I-V plots. To do this, we kept the membrane potential at -70 mV and applied series of 500 ms current injections ranging from -100 pA to 160 pA, at 20 pA increments (Fig. 5A). In a representative neuron, we observed a clear and stable increase in evoked activity after 20 min of photostimulation for lower current steps (40, 60 and 80 pA), with no action potential in the first min with 40 pA, and 3 action potentials, 20 min later with the same current injection. Once the increase in response occurred, it did not change, in either direction, for duration of the recording (3 action potentials after 80 min of photostimulation with 40 pA of current injection) (Figure 5B).

A rise in the excitability could be related to an increase in membrane resistance (Marder and Goaillard, 2006). We used the I-V data with negative current steps to obtain resistance values, before and after photostimulation (Fig. 5C). We observed significant increases in input resistance when comparing the start of the photostimulation (293 $\pm$ 32 mΩ; n = 5, 4 mice) of and 30 min later (361 $\pm$ 30 mΩ; p = 0.0001; student's t test). Meanwhile, resistances measurements in unstimulated neurons between the first minute of IV recording (287 $\pm$ 65 mΩ) and at 30 minutes (286 $\pm$ 55 mΩ) neurons did not show any changes (p = 0.9 student's t test; n = 3, 3 mice; Fig. 5D). We conclude that increases in excitability are associated with increases in membrane resistance.

300 **Photostimulation induces increases in firing rate and frequency**

301 To measure the physiological effect of the detected changes in membrane excitability in the
302 population of photostimulated neurons, we measured firing rate, mean instantaneous frequency
303 and mean frequency between the two first initial spikes for each current step of the I/V protocol,
304 tabulating all parameters for photostimulated neurons and unstimulated procedures in response
305 to each current step. (Table 1).

306 To compare firing rates, we averaged the number of spikes before and after photostimulation for
307 each neuron (Fig. 6 A [left panel]). We found that increases in firing rate always occurred after 15
308 - 20 min of photostimulation at lower current steps (from 40 to 120 pA; n = 7, 5 mice). One of the
309 most noticeable changes was found with 60 pA current steps (before: 2.6 $\pm$ 1 vs. after: 5 $\pm$ 1
310 spikes; p = 0.009; student's t test; n = 7, 5 mice). However, no differences were found for highest
311 current steps (140 and 160 pA; p = 0.1 and 0.2; student's t test; n = 7, 5 mice). Unstimulated
312 neurons did not show differences in firing rate, when we compared the firing rate at minute 1 vs.
313 30 minutes later for each current step (from 40 to 160 pA: $p > 0.05$; student's t test; n = 3, 3 mice)
314 (Fig. 6 A [central panel]). We also found difference in initial firing rate of photostimulated vs.
315 unstimulated neurons (Table 2: for 40 to 80 pA: $p < 0.05$; unpaired student's t test; n = 7, 5 mice
316 for photostimulated neurons and n = 3, 3 mice for unstimulated) (Fig. 6 A [right panel]).

317 Similar results were found when analyzing the mean instantaneous firing frequencies, which also
318 increased after photostimulation. The most significant increases happened with 40 to 80 pA
319 current injection for the before and after comparison (see Table 1; $p < 0.05$; paired student's t
320 test) (Fig. 6 B and C [left panel]). One of the most noticeable changes was with the 60 pA current
321 step (before: 6 $\pm$ 2 versus after: 10 $\pm$ 2.6 Hz; p = 0.007; student's t test; n = 7, 5 mice). Meanwhile,
322 unstimulated neurons did not show significant differences for lower current steps (40, 60 and 100
323 pA; $p > 0.1$; student's t test; n = 3, 3 mice). However, for higher current steps (80,120 to 160 pA)

the mean firing frequency significantly decreased, when compared with the data at the first minute. (e.g. 16 ± 3 at min 1 vs. 15 ± 3 Hz 30 min after, for 120 pA step; $p < 0.05$; student's t test) (Fig. 6 B [central panel]). We also found significant differences of mean frequency between photostimulated and unstimulated neurons for the lowest current steps (40 and 60 pA; see Table 2, $p < 0.01$; unpaired student's t test; n = 7, 5 mice for photostimulated neurons and n = 3, 3 mice for unstimulated) but not for higher current steps (80 to 160 pA; $p > 0.05$; unpaired student's t test) (Fig. 6 B [right panel]).

Finally, to evaluate the modification of firing properties that could facilitate burst induction, we measured the mean frequency of the two first spikes for each current step. Frequency increases occurred with 40 to 80 pA current steps after photostimulation (see Table 1; $p < 0.05$; paired student's t test; n = 7, 5 mice) (Fig. 6 C [left panel]). The clearest change was for 40 pA current steps, where the mean frequency difference between before and after was 5.3 ± 1.5 Hz ($p = 0.001$; paired student's t test). Unstimulated neurons did not show significant differences after 30 minutes of recordings for lower current steps (40 to 140 pA; $p > 0.05$; paired student's t test). Only 160 pA current steps resulted in a significant mean frequency decrease (e.g. 42.5 ± 14 at min 1 vs. 38.5 ± 14 Hz 30 min after; $p = 0.01$; paired student's t test) (Fig. 6 C [central panel]). We found significant changes in mean frequency between photostimulated and unstimulated neurons for lower current steps (40 and 60 pA; see Table 2; $p < 0.01$; unpaired student's t test; n = 7, 5 mice for photostimulated neurons and n = 3, 3 mice for unstimulated), but not for higher current steps (80 to 160 pA; $p > 0.05$; unpaired student's t test) (Fig. 6 C [right panel]). This set of results revealed that photostimulation produced a robust increase in current-dependent firing.

346 **Lowering of firing threshold after photostimulation**

347 Burst firing depends on the interplay between the afterhyperpolarizations (AHPs) and
348 afterdepolarizations (ADPs) that follows the first action potential (Brumberg et al., 2000). To
349 explore this, we evaluated the dynamic of action potentials using phase plot analysis. We used
350 the first spikes from 60 pA current injections in the I-V dataset, because during this current step
351 all neurons displayed action potentials before and after the photostimulation protocol. First, action
352 potentials were detected after setting a threshold of >0.00015 in the first derivative of membrane
353 potential waveform, a value which also corresponds to firing threshold. Voltage vs. time values
354 (mV/ms) were plotted against the membrane potential (mV). In this analysis, action potentials are
355 represented as a loop in which the starting point represents firing threshold (Fig. 7A). The majority
356 of phase plots display a leftward offset, making evident a shift in firing threshold after 30 min of
357 photostimulation (-37 ± 3 before vs. -42.7 ± 3 mV after; p = 0.008; Wilcoxon' test; n = 8, 5 mice).
358 Consistent with this, we found a significant reduction in firing threshold before and after
359 photostimulation (3.5 ± 1 mV; p = 0.0078 by Wilcoxon's test; n = 8 cells, 5 mice). Analogous to
360 long lasting changes in firing rate, the reduction in firing threshold was stable and did not increases
361 more even 40 min after photostimulation protocol (3.7 ± 1 mV after 30 min vs. 4.2 ± 1 after 40
362 min; p = 0.9; Wilcoxon's test; n = 8, 5 mice). Meanwhile, we found no statistically significant
363 differences in firing threshold of unstimulated neurons, when comparing the beginning versus the
364 end of recording (-40 ± 3 and -39 ± 3 mV respectively; p = 0.25; n = 3 cells, 3 mice) (Figure 7B).

365 We also documented a lowering of the threshold voltage when we compared the change in
366 threshold voltage at the first minute (0.4 ± 0.2 mV), 30 min (3.7 ± 1 mV; p = 0.0078) and 40 min
367 (4.2 ± 1 mV; p = 0.03 by Wilcoxon's test; n = 8 cells) for photostimulated cells. Unstimulated
368 neurons displayed no changes (0.6 ± 0.4 mV at the first min vs. -0.8 ± 0.5 mV 30 min later; p =
369 0.25; Wilcoxon's test; n = 3, 3 mice) (Figure 7C). These decreases in threshold for

370 photostimulated neurons were significant, when compared to unstimulated neurons (3.7 ± 1 mV
371 photostim vs. -0.8 ± 0.5 mV unstimulated neurons; p = 0.25; Mann Whitney's test).

372 Altogether, these results indicate that photostimulation significantly increases membrane
373 resistance and lowers firing threshold, which increases action potential firing. These effects nicely
374 explain the increase in neuronal excitability previously observed (Figure 4). Thus,
375 photostimulation could enable weak synaptic inputs to reach firing threshold, facilitating the
376 formation or maintenance of a neuronal ensemble.

377

Discussion

The traditional view of a neuronal ensemble is that it is created by strengthening of its synaptic connections after repeated coactivation (Hebb, 1949; Carrillo-Reid et al., 2016; Hoshiba et al., 2017). However, recent results have questioned whether synaptic plasticity is the unique mechanism of neuronal ensembles formation (Zhang and Linden, 2003; Disterhoft and Oh, 2006; Ryan et al., 2015). Consistent with this, here we describe that the co-photostimulation of pairs of connected or unconnected neurons, the same manipulation that builds an artificial neuronal ensemble *in vivo* (Carrillo-Reid et al., 2016), do not induce detectable changes in synaptic plasticity. Instead, neurons become more active spontaneously after photostimulation, apparently due to increases in membrane resistance and reductions in action potential threshold, as cell-intrinsic mechanisms. Thus, neuronal excitability may increase the efficiency of existing synaptic connections between neurons in an ensemble, without necessarily altering synaptic plasticity.

Role of synaptic mechanisms in ensemble formation

The formation or maintenance of neuronal ensembles have been ascribed to increases in synaptic connectivity (Hebb, 1949; Carrillo-Reid et al., 2016; Hoshiba et al., 2017). Indeed, there is a preferential connectivity between neurons that corresponds with similar receptive fields (Cossell et al., 2015). An increased connectivity also probably underlies pattern completion in cortical ensembles (Carrillo-Reid et al., 2019). Thus, a few strong connections could drive local excitation of the majority of neurons with weak connections (Cossell et al., 2015). Here we mimic *in vitro* previous two-photon optogenetic photostimulation experiments *in vivo* to generate ensembles in layer 2/3 pyramidal cells from mouse primary visual cortex (Carrillo-Reid et al., 2016), and tested whether synaptic mechanisms were involved in ensemble formation. We measured the amplitude

of evoked EPSC and PPR to examine whether synaptic efficiency between two connected neurons had changed (Bliss and Gardner-Medwin, 1973).

Disproving our initial hypothesis, our findings surprisingly indicated a lack of significant changes in synaptic parameters of connected neurons and we did not detect any new connections formed after photostimulation in previously unconnected neurons. Moreover, spontaneous synaptic inputs apparently also remained the same. Although we did not observe significant differences in any case, in spite of changes in synaptic plasticity being our initial hypothesis based on our previous *in vivo* data (Carrillo-Reid et al., 2016), it is possible that the *in vitro* conditions could have obscured these changes. A lack of synaptic plasticity may also be due to a suppression of neurotransmitter release (Fioravante and Regehr, 2011). Certainly, prolonged presynaptic stimulation could induce short-term synaptic depression (Schneggenburger et al., 2002). In any case, the heterogeneity have found in synaptic facilitation and depression, as seen in our data, matches other published reports (Schneggenburger et al., 2002). But because of these negative results, we suspected that mechanisms other than synaptic plasticity could be participating in the artificial ensemble consolidation or formation.

Cell-intrinsic mechanisms of ensemble formation

Indeed, although no changes were observed in synaptic parameters, robust activity-dependent increases in spontaneous firing were easily detected in photostimulated neurons. This was consistent with increases in spontaneous activity observed with calcium signals after photostimulation training *in vivo* (Carrillo-Reid et al., 2016). This suggests that the *in vivo* photostimulation protocol was accurately reproduced in our *in vitro* conditions.

423 An increase in cellular activity through cell-intrinsic mechanisms after prolonged firing is
424 consistent with many functional studies in vertebrates, even under very different experimental
425 protocols. For example: increases in excitability are found following LTP induction in visual cortex
426 (Cudmore and Turrigiano, 2004) or in hippocampal CA1 (Xu, 2005), and after behavior training in
427 CA1 (Disterhoft et al., 1986). Intrinsic excitability is also modified when an animal is exposed to
428 novel sensorial experience (Brown et al., 2019) or after environmental enrichment (Valero-
429 Aracama et al., 2015). Our results reveal an additional paradigm to induce a similar increase in
430 spontaneous activity by direct postsynaptic photostimulation and imply that optogenetic imprinting
431 of ensembles (Carrillo-Reid et al., 2016), increases postsynaptic excitability.

432

433 **Modification of Intrinsic mechanisms by photostimulation**

434 Our data reveal an intensity-dependent and persistent increase in firing rate after
435 photostimulation. This may be due to the increase in membrane resistance and/or the decreases
436 in rheobase that we observed. The synergy between these two mechanisms could make the
437 neuron reach its firing threshold with smaller depolarizations. Thus, an increase in excitability is
438 particularly relevant for lower current injections generated by weaker inputs. We propose that,
439 after photostimulation, neurons shift to a more excitable state, revealing new connections, like an
440 iceberg emerging out of the water (Figure 7). Therefore the same, unchanged synaptic inputs
441 could bring neurons to threshold and induce increased output firing after photostimulation,
442 improving their synaptic efficiency in postsynaptic pyramidal neurons (Zhang and Linden, 2003;
443 Titley et al., 2017; Lisman et al., 2018; Debanne et al., 2019). Neuronal photostimulation would
444 functionally alter the circuit, but without changing the synapses themselves and this phenomenon
445 could occur very rapidly.

446 Modifications in sub- and suprathreshold membrane conductance that initiate an action potential
447 or a burst could underlie increased excitability (Brumberg et al., 2000). In terms of passive
448 properties, our results coincide with many others studies that have shown alterations in input
449 resistance as the mechanism that can be responsible for increases in excitability (Disterhoft et
450 al., 1986; Valero-Aracama et al., 2015; Brown et al., 2019; Pignatelli et al., 2019). Activity-
451 dependent increase in input resistance have been shown in hippocampal neurons, where it has
452 been proposed that the larger increase in excitability could be potentiated by a suppression of G
453 protein-couple inwardly rectifying K^+ channels (GIRK channels) (Valero-Aracama et al., 2015); or
454 by cAMP-responsive element-binding protein (CREB)-dependent control of excitability by
455 reducing K^+ conductance (Yu et al., 2017; Lisman et al., 2018). Moreover, recent studies show
456 that persisting firing could be mediated by an ether-à-gogo related gene (ERG) K^+ channel in
457 neocortical pyramidal neurons (Cui and Strowbridge, 2018; Debanne et al., 2019). In this view,
458 calcium entry induced by repetitive activation could modulate leak potassium currents in the
459 neurons, which will ease their persistent activity.

460 Reported cell-intrinsic mechanisms that induce excitability seem to be cellular-type and perhaps
461 also stimulation protocol-dependent (Angelo et al., 2012). Hence, diverse changes in action
462 potential firing have been identified. One of the most common changes is a reduction in after-
463 hyperpolarization (AHP) amplitude, described in hippocampal neurons (Disterhoft et al., 1986;
464 Zhang and Linden, 2003; Disterhoft and Oh, 2006; Malik and Chattarji, 2012; Pignatelli et al.,
465 2019). Nevertheless, we found a significant decrease in spike threshold as the most robust
466 change in photostimulated neurons. This parameter also determines the firing frequency of
467 neurons associated with voltage-dependent sodium or calcium currents. Changes in threshold
468 appears to be common in cortical neurons after intrinsic plasticity induction (Cudmore and
469 Turrigiano, 2004; Paz et al., 2009), but has also been found in hippocampal neurons (Xu, 2005;
470 Malik and Chattarji, 2012; Valero-Aracama et al., 2015). Consistent with this, visual deprivation

471 increases spike threshold in pyramidal visual cortex, as an example of a mechanism that reduces
472 neuronal excitability (Brown et al., 2019). It has been proposed that a regulation of the persistent
473 sodium current could underlie the lowering of spike threshold, modulated by protein kinase C
474 (Astman et al., 1998; Valero-Aracama et al., 2015), or protein kinase A activation-dependent of
475 calcium influx (Cudmore and Turrigiano, 2004). Therefore, the intrinsic plasticity by optogenetic
476 photostimulation that we report in L2/3 pyramidal neurons from visual cortex could result from
477 modifications of voltage-gated ion channels and inward rectification by potassium channels.
478 Future studies will examine the exact molecular mechanisms underlying these increases in
479 excitability.

480

481 **Intrinsic excitability in neuronal ensembles formation**

482 Many studies have shown that Hebbian plasticity is required for intrinsic plasticity induction
483 (Debanne et al., 2019). Thus, NMDA receptor activation is necessary to increase firing probability
484 in neurons (Disterhoft et al., 1986; Cudmore and Turrigiano, 2004; Xu, 2005; Malik and Chattarji,
485 2012; Kim et al., 2016; Pignatelli et al., 2019). Behavioral training also induce neuronal excitability
486 through Hebbian mechanisms (Disterhoft et al., 1986; Malik and Chattarji, 2012; Valero-Aracama
487 et al., 2015). Other studies, agreeing with our results, have demonstrated that for increasing
488 neuronal excitability, postsynaptic stimulation could be enough to improve synaptic efficiency
489 (Stackman et al., 2002; Paz et al., 2009).

490 Our work provides evidence that supports the relevance of intrinsic mechanisms induced by
491 photostimulation training in neuronal ensemble formation. The possibility to change the output
492 pattern of a postsynaptic neuron through the modification of its firing properties could be a factor
493 that promotes synaptic efficacy (Lisman, 1997; Brumberg et al., 2000). Thus, fast plasticity in

intrinsic excitability could have a major impact on network dynamics and could serve as an important information-storage mechanism which may contribute to memory formation (Xu, 2005; Marder and Goaillard, 2006; Lisman et al., 2018; Pignatelli et al., 2019) and to the generation of intrinsic circuit states, such as ensembles and attractors (Hopfield, 1982; Buzsáki, 2010; Miller et al., 2014b; Carrillo-Reid et al., 2016, 2019).

References

Abeles M (1991) Corticonics. Cambridge University Press.

Abraham WC, Jones OD, Glanzman DL (2019) Is plasticity of synapses the mechanism of long-term memory storage? npj Sci Learn 4:9.

Angelo K, Rancz EA, Pimentel D, Hundahl C, Hannibal J, Fleischmann A, Pichler B, Margrie TW (2012) A biophysical signature of network affiliation and sensory processing in mitral cells. Nature 488:375–378.

Astman N, Gutnick MJ, Fleidervish IA (1998) Activation of Protein Kinase C Increases Neuronal Excitability by Regulating Persistent Na + Current in Mouse Neocortical Slices. J Neurophysiol 80:1547–1551.

Bliss TVP, Gardner-Medwin AR (1973) Long-lasting potentiation of synaptic transmission in the dentate area of the unanaesthetized rabbit following stimulation of the perforant path. J Physiol 232:357–374.

Brown APY, Cossell L, Margrie TW (2019) Visual Experience Regulates the Intrinsic Excitability of Visual Cortical Neurons to Maintain Sensory Function. Cell Rep 27:685-689.e4.

Brumberg JC, Nowak LG, McCormick DA (2000) Ionic Mechanisms Underlying Repetitive High-Frequency Burst Firing in Supragranular Cortical Neurons. J Neurosci 20:4829–4843.

Buzsáki G (2010) Neural syntax: cell assemblies, synapsembles, and readers. Neuron 68:362–385.

Carrillo-Reid L, Han S, Yang W, Akrouh A, Yuste R (2019) Controlling Visually Guided Behavior by Holographic Recalling of Cortical Ensembles. Cell 178:447-457.e5.

Carrillo-Reid L, Yang W, Bando Y, Peterka DS, Yuste R (2016) Imprinting and recalling cortical ensembles. Science (80-) 353:691–694.

Churchland PS, Sejnowski TJ (1992) The computational brain. Cambridge, MA, US: The MIT Press.

Cossart R, Aronov D, Yuste R (2003) Attractor dynamics of network UP states in the neocortex. Nature 423:283–288.

Cossell L, Iacaruso MF, Muir DR, Houlton R, Sader EN, Ko H, Hofer SB, Mrsic-Flogel TD (2015) Functional organization of excitatory synaptic strength in primary visual cortex. Nature 518:399–403.

530 Cudmore RH, Turrigiano GG (2004) Long-Term Potentiation of Intrinsic Excitability in LV Visual
531 Cortical Neurons. J Neurophysiol 92:341–348.

532 Cui ED, Strowbridge BW (2018) Modulation of Ether-à-Go-Go Related Gene (ERG) Current
533 Governs Intrinsic Persistent Activity in Rodent Neocortical Pyramidal Cells. J Neurosci
534 38:423–440.

535 Debanne D, Inglebert Y, Russier M (2019) Plasticity of intrinsic neuronal excitability. Curr Opin
536 Neurobiol 54:73–82.

537 Disterhoft JF, Coulter DA, Alkon DL (1986) Conditioning-specific membrane changes of rabbit
538 hippocampal neurons measured *in vitro*. Proc Natl Acad Sci 83:2733–2737.

539 Disterhoft JF, Oh MM (2006) Learning, aging and intrinsic neuronal plasticity. Trends Neurosci
540 29:587–599.

541 Fioravante D, Regehr WG (2011) Short-term forms of presynaptic plasticity. Curr Opin
542 Neurobiol 21:269–274.

543 Hamm JP, Peterka DS, Gogos JA, Yuste R (2017) Altered Cortical Ensembles in Mouse Models
544 of Schizophrenia. Neuron 94:153-167.e8.

545 Hebb DO (1949) The Organization of Behavior, New York: Wiley.

546 Hopfield JJ (1982) Neural networks and physical systems with emergent collective
547 computational abilities. Proc Natl Acad Sci U S A 79:2554–2558.

548 Hoshiba Y, Wada T, Hayashi-Takagi A (2017) Synaptic Ensemble Underlying the Selection and
549 Consolidation of Neuronal Circuits during Learning. Front Neural Circuits 11.

550 Johansson F, Jirenhed D-A, Rasmussen A, Zucca R, Hesslow G (2014) Memory trace and
551 timing mechanism localized to cerebellar Purkinje cells. Proc Natl Acad Sci 111:14930–
552 14934.

553 Kim T, Oh WC, Choi JH, Kwon H-B (2016) Emergence of functional subnetworks in layer 2/3
554 cortex induced by sequential spikes *in vivo*. Proc Natl Acad Sci 113:E1372–E1381.

555 Ko H, Hofer SB, Pichler B, Buchanan KA, Sjöström PJ, Mrsic-Flogel TD (2011) Functional
556 specificity of local synaptic connections in neocortical networks. Nature 473:87–91.

557 Lisman J, Cooper K, Sehgal M, Silva AJ (2018) Memory formation depends on both synapse-
558 specific modifications of synaptic strength and cell-specific increases in excitability. Nat
559 Neurosci 21:309–314.

Lisman JE (1997) Bursts as a unit of neural information: making unreliable synapses reliable. Trends Neurosci 20:38–43.

Lorente de Nó R (1933) Studies on the structure of the cerebral cortex. I. The area entorhinalis. J für Psychol und Neurol.

Lorente De Nó R (1938) Analysis of the activity of the chains of internuncial neurons. J Neurophysiol 1:207–244.

Malik R, Chattarji S (2012) Enhanced intrinsic excitability and EPSP-spike coupling accompany enriched environment-induced facilitation of LTP in hippocampal CA1 pyramidal neurons. J Neurophysiol 107:1366–1378.

Marder E, Goaillard J-M (2006) Variability, compensation and homeostasis in neuron and network function. Nat Rev Neurosci 7:563–574.

Mardinly AR, Oldenburg IA, Pégard NC, Sridharan S, Lyall EH, Chesnov K, Brohawn SG, Waller L, Adesnik H (2018) Precise multimodal optical control of neural ensemble activity. Nat Neurosci 21:881–893.

Marshel JH, Kim YS, Machado TA, Quirin S, Benson B, Kadmon J, Raja C, Chibukhchyan A, Ramakrishnan C, Inoue M, Shane JC, McKnight DJ, Yoshizawa S, Kato HE, Ganguli S, Deisseroth K (2019) Cortical layer-specific critical dynamics triggering perception. Science 365.

Miller J -e. K, Ayzenshtat I, Carrillo-Reid L, Yuste R (2014a) Visual stimuli recruit intrinsically generated cortical ensembles. Proc Natl Acad Sci 111:E4053–E4061.

Miller JK, Ayzenshtat I, Carrillo-Reid L, Yuste R (2014b) Visual stimuli recruit intrinsically generated cortical ensembles. Proc Natl Acad Sci U S A 111:E4053-61.

Paz JT, Mahon S, Tiret P, Genet S, Delord B, Charpier S (2009) Multiple forms of activity-dependent intrinsic plasticity in layer V cortical neurones *in vivo*. J Physiol 587:3189–3205.

Pignatelli M, Ryan TJ, Roy DS, Lovett C, Smith LM, Muralidhar S, Tonegawa S (2019) Engram Cell Excitability State Determines the Efficacy of Memory Retrieval. Neuron 101:274-284.e5.

Ryan TJ, Roy DS, Pignatelli M, Arons A, Tonegawa S (2015) Engram cells retain memory under retrograde amnesia. Science (80-) 348:1007–1013.

Schneggenburger R, Sakaba T, Neher E (2002) Vesicle pools and short-term synaptic depression: lessons from a large synapse. Trends Neurosci 25:206–212.

Schüz A, Braitenberg V (2001) Cerebral Cortex: Organization and Function. In: International Encyclopedia of the Social & Behavioral Sciences, pp 1634–1640. Elsevier.

Shepherd GM (2004) The Synaptic Organization of the Brain (Shepherd GM, ed). Oxford University Press.

Stackman RW, Clark AS, Taube JS (2002) Hippocampal spatial representations require vestibular input. Hippocampus 12:291–303.

Ting JT, Lee BR, Chong P, Soler-Llavina G, Cobbs C, Koch C, Zeng H, Lein E (2018) Preparation of Acute Brain Slices Using an Optimized N-Methyl-D-glucamine Protective Recovery Method. J Vis Exp:e53825.

Titley HK, Brunel N, Hansel C (2017) Toward a Neurocentric View of Learning. Neuron 95:19–32.

Tonegawa S, Pignatelli M, Roy DS, Ryan TJ (2015) Memory engram storage and retrieval. Curr Opin Neurobiol 35:101–109.

Valero-Aracama MJ, Sauvage MM, Yoshida M (2015) Environmental enrichment modulates intrinsic cellular excitability of hippocampal CA1 pyramidal cells in a housing duration and anatomical location-dependent manner. Behav Brain Res 292:209–218.

Xu J (2005) Activity-Dependent Long-Term Potentiation of Intrinsic Excitability in Hippocampal CA1 Pyramidal Neurons. J Neurosci 25:1750–1760.

Yu X-W, Oh MM, Disterhoft JF (2017) CREB, cellular excitability, and cognition: Implications for aging. Behav Brain Res 322:206–211.

Yuste R (2015) From the neuron doctrine to neural networks. Nat Rev Neurosci 16:487–497.

Zhang W, Linden DJ (2003) The other side of the engram: experience-driven changes in neuronal intrinsic excitability. Nat Rev Neurosci 4:885–900.

Table 1. Comparation of parameters associated with membrane excitability in intensity-depended response, for photostimulated and unstimulated neurons.

	Number of spikes			Mean instant firing frequencies (Hz)			Mean frequencies of two first spikes (Hz)		
pA	Before	After	P Value	Before	After	P Value	Before	After	P Value
Photostimulated neurons									
20	0.0	0.0	-	0.0	0.0	-	0.0	0.0	-
40	0 ± 0.07	2 ± 1	0.01 **	0	7 ± 1.9	0.001 ***	0 ± 0	7.4 ± 2	0.001 ***
60	2.6 ± 1	5 ± 1	0.009 **	6 ± 2	10 ± 2.6	0.007 **	7 ± 3	14 ± 6	0.006 **
80	5 ± 1	7 ± 0.8	0.009 **	11 ± 2.8	14.6 ± 3	0.04 *	14 ± 6	21 ± 8	0.05 *
100	7 ± 2	8 ± 0.8	0.03 *	15.4 ± 3	17.4 ± 3	0.06	25 ± 11	29.4 ± 15	0.1
120	8 ± 1.3	9 ± 1	0.04 *	18 ± 4.6	20 ± 3.7	0.3	37 ± 20	36.6 ± 18	0.9
140	9 ± 1.6	10.4 ± 1	0.1	22 ± 4	23 ± 3	0.6	51 ± 22	49 ± 21	0.6
160	9.8 ± 1	11 ± 0.5	0.2	24.2 ± 5	24.8 ± 4	0.7	57 ± 28	57 ± 28	0.9
Unstimulated neurons									
20	0.0	0.0	-	0.0	0.0	-	0.0	0.0	-
40	1 ± 2	1 ± 2	1	2.4 ± 4.2	2.2 ± 3.8	0.4	2.7 ± 5	2.4 ± 4	0.4
60	3 ± 2	2 ± 2	0.4	5.7 ± 5.7	4.8 ± 5	0.2	7 ± 8	6 ± 7	0.2
80	5 ± 2	4 ± 2	1	10 ± 4	9.3 ± 4.4	0.03 *	14 ± 7.4	12.4 ± 7	0.02 *
100	6 ± 2	6 ± 1.5	0.4	13.6 ± 4	13 ± 4.7	0.3	20 ± 8.6	21 ± 11.6	0.8
120	7 ± 1.8	6.3 ± 2	0.2	16 ± 5	15 ± 5	0.03 *	28.6 ± 15	24.7 ± 13	0.1
140	8 ± 2	7.7 ± 2	0.4	19 ± 5.5	16.7 ± 6	0.02 *	35 ± 20.5	32 ± 21	0.2
160	9 ± 2	8.3 ± 2	0.2	21 ± 6	19 ± 7	0.03 *	43 ± 25	39 ± 24.6	0.01 **

616

617 **Table 1.** Firing rate at minute 1 vs. 30 minutes later for each current step for the number of spikes,
618 mean instant firing frequencies, mean frequencies of two first spikes. Comparation to determine
619 the change in intensity-depended response in photostimulated (n = 7, 5 mice) and unstimulated
620 condition (n = 3, 3 mice). Data represent mean ± SEM. *p < 0.05, **p < 0.01 and ***p < 0.001 by
621 student's t test.

Table 2. Comparation of the changes in intensity-depended response for photostimulated vs. unstimulated neurons.

	Number of spikes			Mean instant firing frequencies (Hz)			Mean frequencies of two first spikes (Hz)		
pA	Photostim	Unstim	P Value	Photostim	Unstim	P Value	Photostim	Unstim	P Value
20	0.0	0.0	-	0.0	0.0	-	0.0	0.0	-
40	1.9 ± 1	0 ± 0	0.04 *	7 ± 0.4	-0.2 ± 2	0.0006 ***	-0.3 ± 0.5	7.4 ± 2	0.0006 ***
60	2.3 ± 2	-0.3 ± 0.5	0.02 *	3.4 ± 0.8	-1 ± 2	0.009 **	-1 ± 1	4.7 ± 2.5	0.007 **
80	2 ± 1	-1 ± 0	0.007 **	3.7 ± 0.3	-1 ± 4	0.07	-1.5 ± 0.3	6.8 ± 7.3	0.09
100	1 ± 1	-0.3 ± 0.5	0.06	2 ± 1	-0.8 ± 2.3	0.08	0.7 ± 5.5	4.3 ± 6.4	0.4
120	1 ± 1	-0.6 ± 0.5	0.02 *	1.5 ± 0.3	-1 ± 3	0.1	-3.9 ± 2.6	-0.3 ± 8.5	0.5
140	1.2 ± 1	-0.3 ± 0.5	0.1	0.6 ± 0.6	-2 ± 2.7	0.1	-3 ± 3.1	-2.5 ± 9.7	0.9
160	1 ± 1	-0.6 ± 0.5	0.1	0.5 ± 0.5	-2 ± 3.2	0.2	-4 ± 0.7	-0.4 ± 10	0.5

Table 2. Mean differences, at the first minute and 30 minutes after, for the number of spikes, mean instant firing frequencies, mean frequencies of two first spikes. Comparation of the changes in the intensity-depended for photostimulated response (n = 7, 5 mice) vs. unstimulated condition (n = 3, 3 mice). Data represent mean ± SEM. *$p < 0.05$, **$p < 0.01$ and ***$p < 0.001$ by unpaired student's t test.

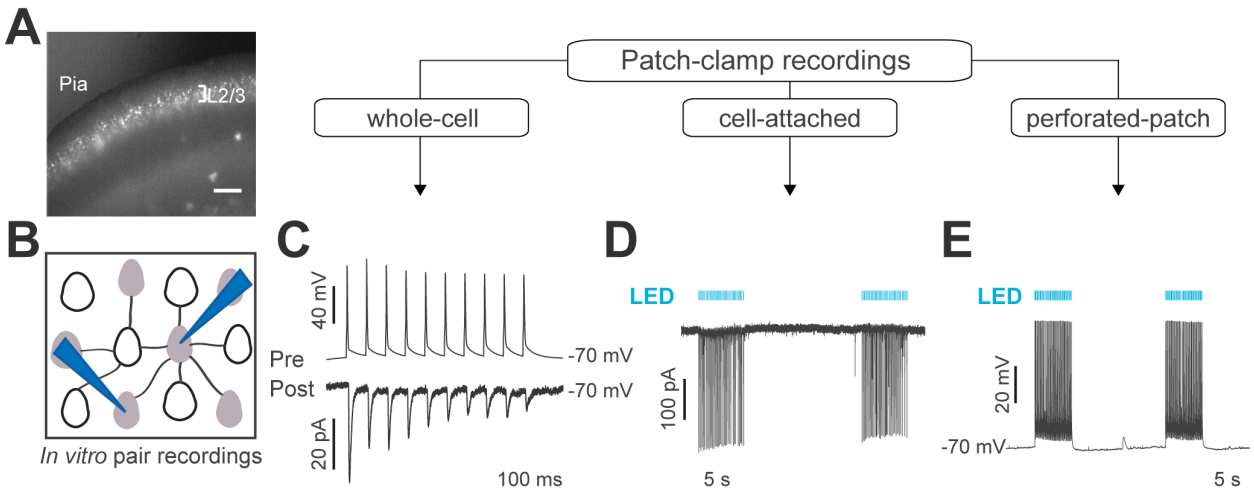

Figure 1. Experimental design.

(**A**). Example image of Ruby3 reporter fluorescent of ST-ChroMe opsin expression in L2/3 pyramidal neurons in primary visual cortex. Sagittal brain slices were obtained from virus injected mice. Scale bar: 200 μM. (**B**) Illustration of *In vitro* pair recording for evaluating monosynaptic connectivity between neurons. (**C**) Whole-cell recording of presynaptic action potentials elicited by 20 Hz train of 10 current injections (2 ms each), followed by the identification of a monosynaptic connection, with postsynaptic currents corresponding to presynaptic spikes. (**D**) Cell-attached and perforated current-clamp recording (**E**) at the beginning of direct optogenetic photostimulation protocol: 1 to 40 min of 10 Hz train, 5 ms light pulses for 4 s followed by 10 s of rest.

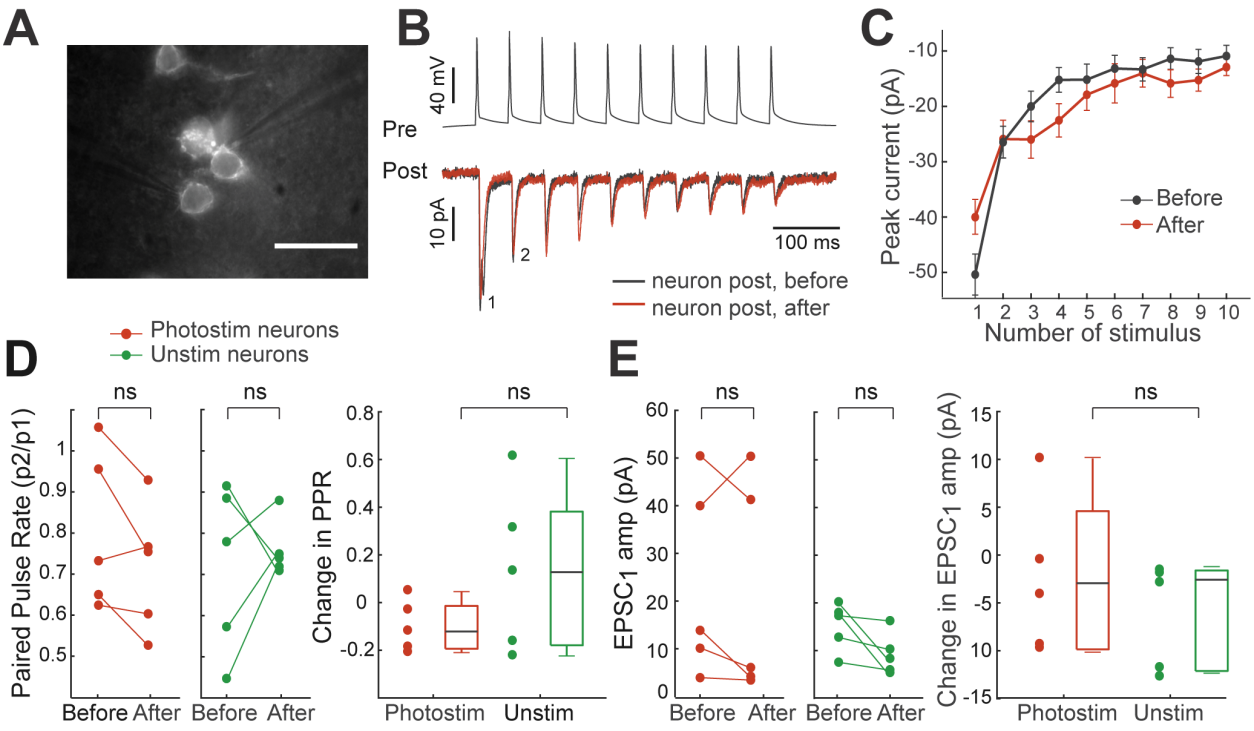

641

642

643 **Figure 2. Lack of effect of photostimulation on evoked synaptic inputs**

644 (**A**) Paired whole-cell recording of presynaptic and postsynaptic neurons during photostimulation.
645 Fluorescent reporter expression of ST-ChroMe opsin in pyramidal neurons L2/3 of primary visual
646 cortex from a mouse brain slice (p40). Scale bar: 40 μM. (**B**) Representative paired recording of
647 synaptically connected neurons. Top: current-clamp recording of presynaptic action potentials in
648 response to 10 pulses (2 ms each) at 20 Hz of current injection. Bottom: voltage-clamp recording
649 of evoked EPSCs before (black) and after (red) 40 min of photostimulation. Each trace is the
650 average of 30 successive responses evoked by presynaptic electrical stimulation. (**C**) Amplitude
651 of evoked EPSCs remain unchanged after optogenetic photostimulation. Average amplitude of
652 30 successive EPSCs evoked in the representative neuron in B, before (black) and after (red)
653 photostimulation. p = 0.7 by Student's t test. Data represent mean ± SEM. (**D**) Mean Paired Pulse
654 Ratio (PPR) remains unchanged before and after photostimulation (red; p = 0.2 by Wilcoxon's
655 test; n = 5 cells, 4 mice) and unstimulated neurons (green; p = 0.7 by Wilcoxon's test, n = 5 cells,

656 3 mice). Right: comparison of change in mean PPRs plotted raw and as a box and whisker plot.
657 p = 0.5 by Mann Whitney's test; n = 5 cells per group. (**E**) Mean $EPSC_1$ amplitude without
658 significant changes before and after photostimulation protocol (red; p = 0.6 by Wilcoxon's test; n
659 = 5 cells) and unstimulated neurons (green; p = 0.06 by Wilcoxon's test, n = 5 cells). Right,
660 comparison of change in mean $EPSC_1$ amplitudes plotted raw and as a box and whisker plot. p =
661 0.5 by Mann Whitney's test; n = 5 cells per group.
662

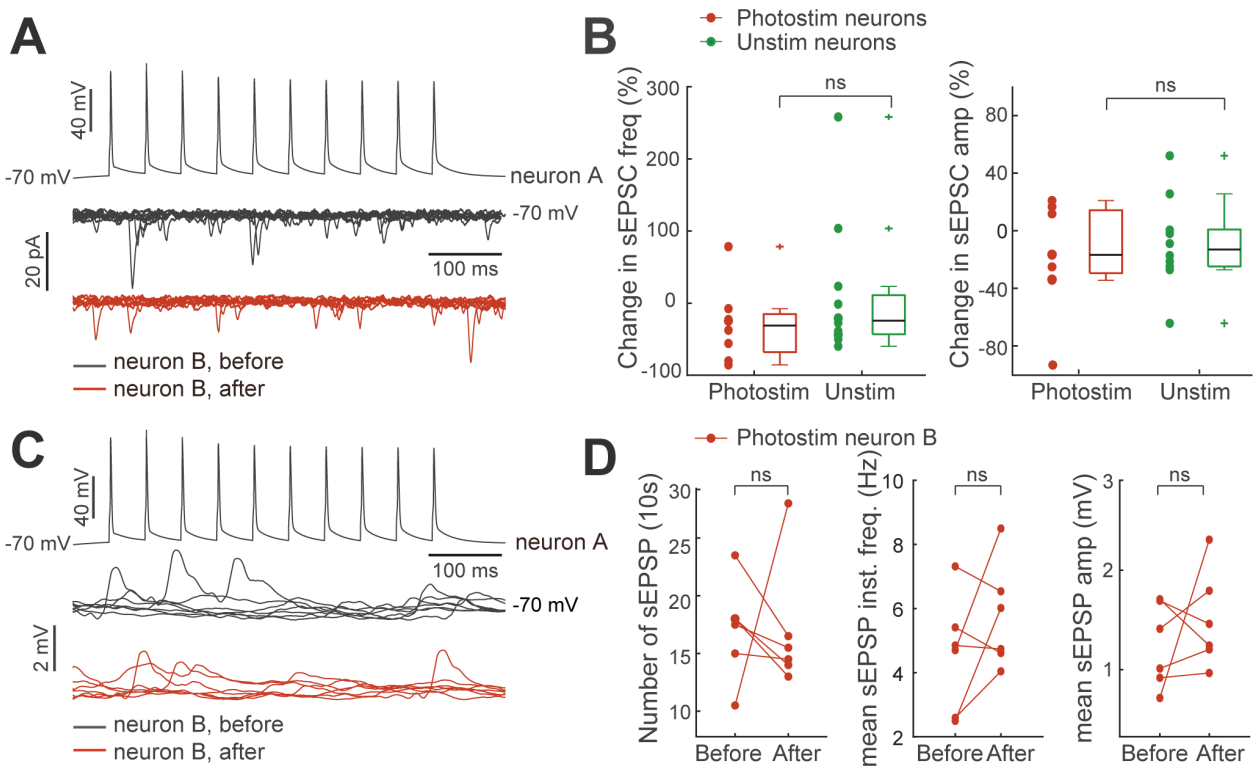

Figure 3. Lack of effect of photostimulation on spontaneous synaptic inputs

(**A**) Representative paired whole-cell recording of non-connected neurons. Spontaneous EPSCs remained unchanged after optogenetic photostimulation. Top: current-clamp recording of presynaptic action potentials in response to 20 Hz-train current injection (neuron A). Bottom: voltage-clamp recording of 10 successive traces of spontaneous EPSCs without presynaptic spike's correspondence (neuron B), before (black) and after (red) 40 min of photostimulation protocol. (**B**) Spontaneous EPSCs frequencies of unstimulated and photostimulated neurons. Change correspond to: the numerical subtraction among the first minute of EPSCs frequency and 40 min after. Photostimulated neurons: red raw and box plot; neurons without photostimulation: green raw and box plot (p = 0.4 by Mann Whitney's test; n = 8 for unstimulated neurons and n = 12 for photostimulated). Right: same as left but for spontaneous EPSC amplitudes. p = 0.9 by Mann Whitney's test. (**C**) Same as A but in current-clamp perforated patch clamp recording of spontaneous EPSPs. (**D**) No significant difference in the number of spontaneous EPSPs, mean

678 of instantaneous frequency and mean of amplitudes, before and after 40 min of photostimulation
679 protocol. Number of spontaneous EPSPs: $p = 0.4$; Instantaneous frequency average: $p = 0.4$;
680 Amplitudes average: $p = 0.7$. Each by Wilcoxon's test; $n = 6$ photostimulated cells.
681

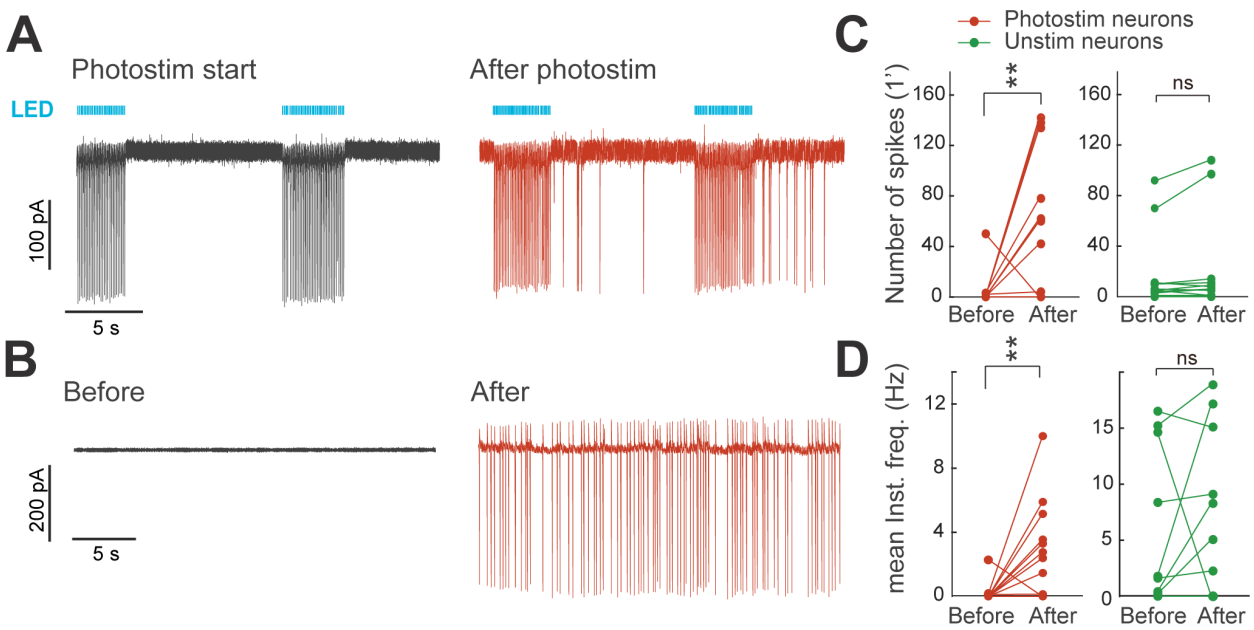

682

683

684 **Figure 4. Spontaneous firing rate increases after photostimulation**

685 (**A**) Neurons increase spontaneous firing after direct optogenetic photostimulation.
686 Representative cell-attached recording of a L2/3 pyramidal neuron that expressed ST-ChroMe
687 opsin. Left: black trace shows at the beginning of photostimulation protocol; blue lines indicated
688 when the LED was ON. Right: red trace shows recording of the same cell after 30 min of
689 photostimulation. (**B**) Spontaneous firing rate recording before (black trace) and after (red trace)
690 30 min of photostimulation. 60 % of the cells increased their spontaneous activity (firing rate) in
691 response to the stimulation protocol and 40 % did not show changes, or instead showed a
692 decrease in activity; n = 17. (**C**) Number of spikes increased after photostimulation. Left:
693 comparing spontaneous firing rate before and after 30 min of photostimulation (red; **p < 0.01 by
694 Wilcoxon's test; n = 17 cells). Right: comparing spontaneous firing rate before and after 30 min
695 without photostimulation (green; p = 0.2 by Wilcoxon's test; n = 13 cells). (**D**) Same as in **C** but
696 for instantaneous frequency of photostimulated neurons (**p < 0.01 by Wilcoxon's test; n = 17
697 cells) and unstimulated neurons (p = 0.3 by Wilcoxon's test; n = 13 cells).

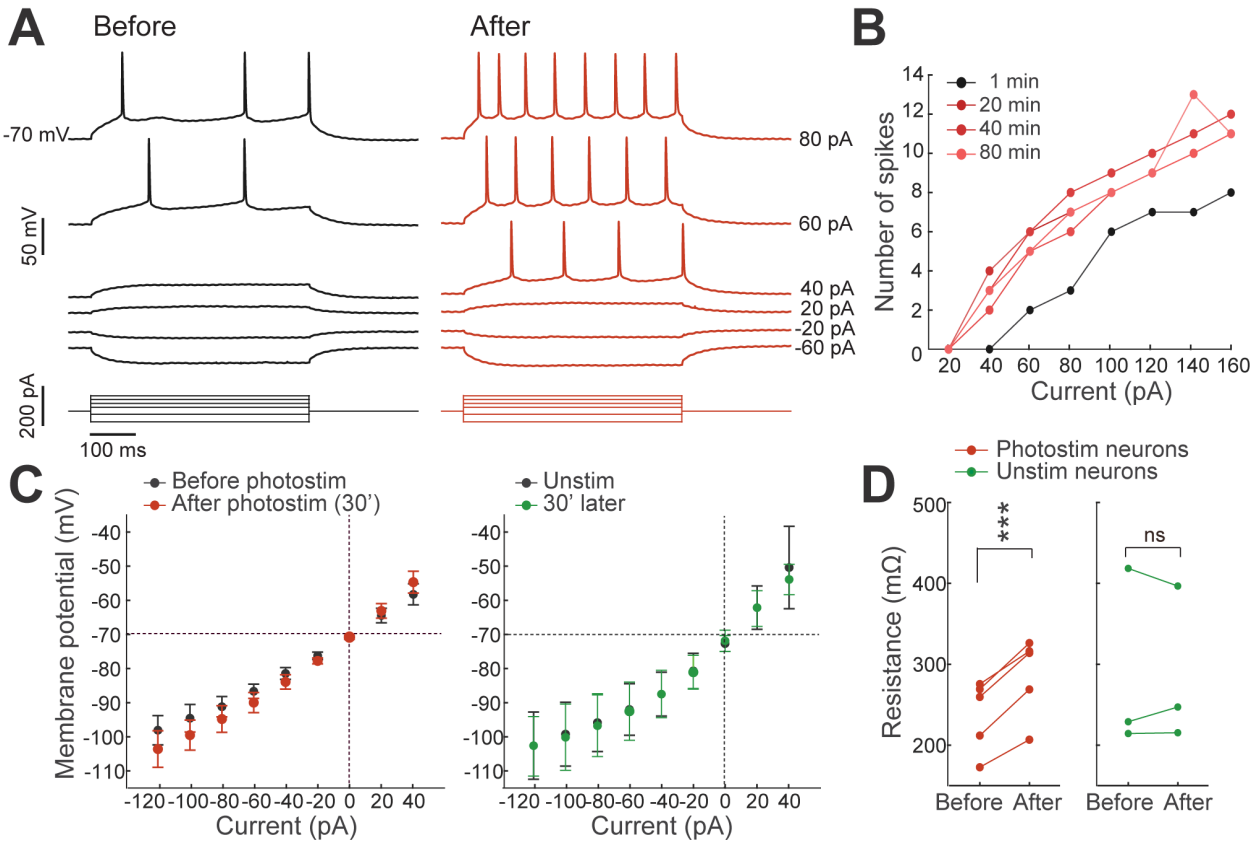

698

699

700 **Figure 5. Membrane input resistance increases after photostimulation**

701 **(A)** Membrane potential excitability increases after photostimulation. Representative membrane
702 voltage recordings with perforated patch-clamp (top) in response 500 ms series of current steps
703 (bottom). Black traces show the membrane potential changes before photostimulation and red
704 traces after 40 min. (**B**) Decrease in the rheobase after 20 min of photostimulation. Number of
705 spikes in response to current steps of a representative photostimulated neuron, before
706 photostimulation (at min 1): the action potentials were not evoked until 60 pA of current injection
707 (black), after 20 min of photostimulation, neurons started to show action potentials at 40 pA of
708 current injection. (**C**) IV plot show the relation between current injection and the membrane
709 potential (Ohm's law: Resistance = V/I). IV curves showed a modification in voltage membrane
710 when we compared before and after 30 min of photostimulation (right graph). This change was
711 not observed in the IV curves of unstimulated neurons (on the left). (**D**) Membrane resistance

712 increases after photostimulation. ***$p < 0.001$ by student's t test; n = 5 cells, 4 mice. Unstimulated
713 neurons remained the same at minute 1 and 30 minutes after ($p = 0.9$ by student's t test; n = 3,
714 3 mice).
715

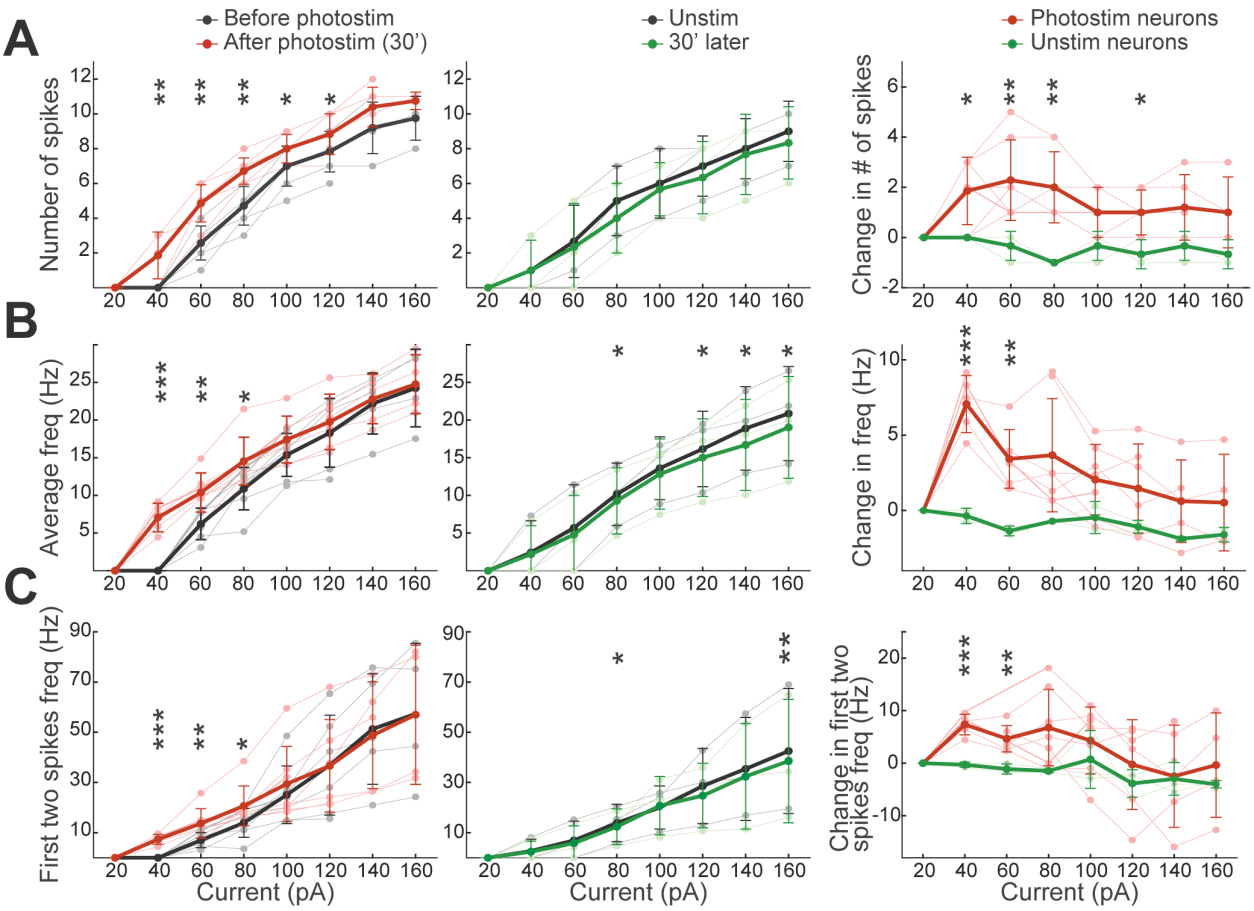

716

717 **Figure 6. Neuronal excitability increases after photostimulation**

718 (**A**) Neuronal activity is increased after photostimulation for the lowest current steps. The thickest
719 lines are average spikes of all neurons before (black) and after (red) photostimulation. Center:
720 average spikes of unstimulated neurons, black line corresponds to first minute and green line to
721 30 minutes after. *p < 0.05 and **p < 0.01 by student's t test. Right: numerical subtraction among
722 the number of spikes in the first minute and 30 minutes after, photostimulated (red) and
723 unstimulated neurons (green). *p < 0.05, **p < 0.01 by unpaired student's t test; n = 7 for
724 photostimulated neurons and n = 3 unstimulated neurons. Data represent mean ± SEM. (**B**) Mean
725 instant frequency increased for 40 to 80 pA of current steps after photostimulation. Same as **A**
726 but for average of instantaneous frequency. *p < 0.05, **p < 0.01 and ***p < 0.001 by student's t
727 test. Right: numerical subtraction among instantaneous frequency in the first minute and 30 min
728 after: *p < 0.05, **p < 0.01 and ***p < 0.001 by unpaired student's t test. (**C**) Frequency of the first

two action potentials increased through 40 to 80 pA of current steps after photostimulation. Same as **A** but for the average of first two action potentials frequency. *$p < 0.05$, **$p < 0.01$ and ***$p < 0.001$ by student's t test. Right: Numerical subtraction among first two action potentials frequency in the first minute and 30 min after: *$p < 0.05$, **$p < 0.01$ and ***$p < 0.001$ by unpaired student's t test.

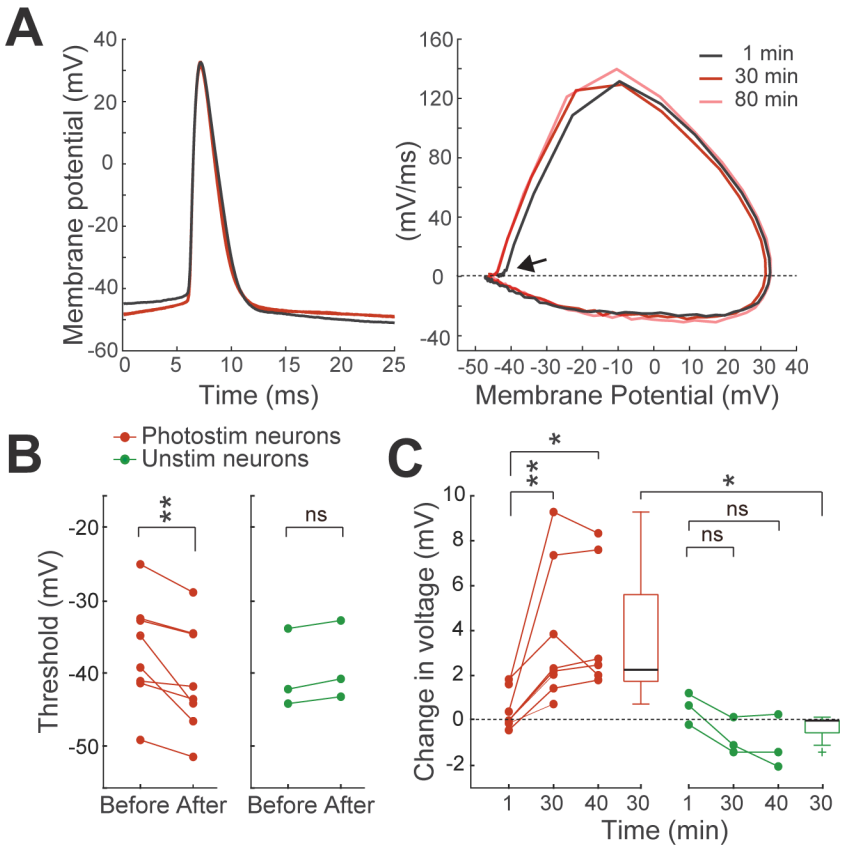

735

736

737 **Figure 7. Spike threshold decreases after photostimulation**

738 (**A**) Firing threshold shifts to more negative potentials after photostimulation. First action potentials
739 from recording under 60 pA steps before (black) and after (red) 30 min of photostimulation, aligned
740 to their firing threshold. Right: Phase plot of action potentials: before start stimulation protocol
741 (black), after 30 min (red) and after 80 min (orange). Arrow shows the firing threshold position.
742 (**B**) Firing threshold was detected for every cell before and after photostimulation, red paired dot
743 plot (**p < 0.01 by Wilcoxon's test; n = 8 cells). Right: unstimulated neurons, green paired dot plot
744 (p = 0.3 by Wilcoxon's test; n = 3 cells). (**C**) Voltage threshold change correspond to: numerical
745 subtraction among two values firing threshold taken in the first min before photostimulation; then,
746 numerical subtraction among first minute firing threshold and 30 min and 40 min later, red data
747 (*p = 0.05 and **p = 0.01 by Wilcoxon's test; n = 8 cells). Likewise, for unstimulated neurons,
748 green data (p = 0.25 by Wilcoxon's test; n = 3 cells). Photostimulated neurons: red box plot and

749 for unstimulated neurons: green box plot. (*$p < 0.05$ by Mann Whitney's test; $n = 8$ for
750 photostimulated and $n = 3$ for unstimulated cells).
751

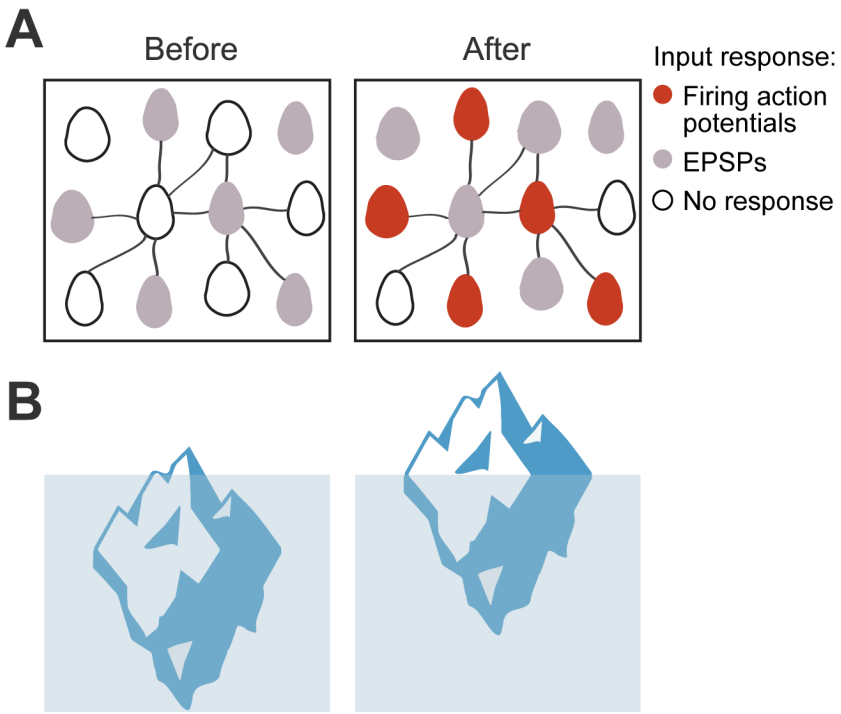

Figure 8. Iceberg emergence model of ensemble formation.

(**A**) Emergence of ensembles after increases in neuronal excitability. Illustration of a diversity in responses to an input of a neuronal population, before and after coactivation (or photostimulation in the case of this study). Color corresponds to membrane potential in response to an input: white are resting membrane potentials, gray are subthreshold responses and red are suprathreshold ones, with firing of action potentials. After photostimulation neurons are more excitable, so the same inputs induce some of them to fire (red cells).

(**B**) Left: Iceberg emergence model: An iceberg with higher density keeps mostly underwater. (Right) But if its density decreases, the iceberg emerges above water. Density is an intrinsic property, and, by changing it, the iceberg changes its response to the same environment. Likewise, for a neuronal ensemble, membrane resistance and firing threshold are neuronal intrinsic property that are being modified, and they enhance its response to the same excitatory input intensity, resulting in an increase depolarization and action potentials.